Chinese Chemical Letters 34 (2023) 107717

Contents lists available at ScienceDirect

Chinese Chemical Letters

journal homepage: www.elsevier.com/locate/cclet

Hierarchically structured flower-like Ru nanoparticles-cucurbit[6]uril/multiwalled carbon nanotubes as efficient pH-universal hydrogen evolution electrocatalyst

Xiali Xiong[a,b], Wei Geng[a], Minna Cao[a,c,*], Rong Cao[a,c,d,*]

[a] State Key Laboratory of Structural Chemistry, Fujian Institute of Research on the Structure of Matter, Chinese Academy Sciences, Fuzhou 350002, China
[b] College of Chemistry Engineering, Fuzhou University, Fuzhou 350108, China
[c] University of Chinese Academy of Sciences, Beijing 100049, China
[d] Fujian Science & Technology Innovation Laboratory for Optoelectronic Information of China, Fuzhou 350108, China

ARTICLE INFO

Article history:
Received 11 July 2022
Accepted 30 July 2022
Available online 2 August 2022

Keywords:
Ruthenium
Cucurbit[n]uril
Hierarchical structure
Hydrogen evolution reaction
pH-universal

ABSTRACT

Developing efficient and stable electrocatalyst to hydrogen evolution reaction adaptable for electrolytes with different pH is a big challenge. In this work, a hierarchically structured ternary nanohybrid composed of flower-like Ru nanoparticles, rigid macrocyclic cucurbit[6]uril (CB[6]) and carboxylated multiwalled carbon nanotubes (MWCNTs) was successfully prepared by chemical wet method. Benefited by the structural merits of flower-like Ru nanoparticles exposed abundant active sites supported by the MWCNTs holding superior mass transport and electrons transfer ability as well as the existence of CB[6], the obtained catalyst exhibited outstanding HER activities with overpotentials of 27, 37 and 70 mV at $-10\ mA/cm^2$ in alkaline, acidic, and neutral electrolytes, respectively. Under the same electrocatalytic operation conditions, the HER performance is comparable or superior to commercial Pt/C catalyst (47, 27 and 49 mV). Besides, chronopotentiometric and accelerated stability test also revealed its extraordinary stability, which could be further employed for electrocatalytic procedure in a broad pH range.

Hydrogen, an alternative fuel for fossil fuels, has been identified as the clean energy source that could realize net-zero emissions in the future [1–3]. Among existing hydrogen production technologies, electrochemical hydrogen evolution reaction (HER) is an environmentally friendly and sustainable approach for high-purity hydrogen production [4–6]. Pt-based electrocatalysts are the state-of-the-art electrocatalysts with excellent HER activity in a wide pH ranges, but the large-scale commercialization is limited by its high price and scarcity [7]. Although great efforts have been devoted to developing non-noble metal materials for HER, such as transition metal carbides [8], transition metal phosphides [9] and single-atom catalysts [10], the activity and stability of non-noble metal catalysts are still far from satisfactory compared with Pt-based catalysts [11], because of the high energy barrier of water dissociation and the difficulty of desorption hydrogen in alkaline media [12]. Therefore, the development of efficient and stable HER catalysts under pH-universal conditions is still a significant challenge, especially for industrial alkaline conditions.

Ru is one of the preferred alternatives to Pt and has attracted much attention in the field of electrocatalytic hydrolysis for its similar hydrogen bond energy to Pt [13], a cheap price (only 1/5 of Pt) and high HER activity for wide pH ranges [14]. Although great efforts have been made, the activity and stability of Ru-based nanomaterials need to be optimized for practical application. An efficient and typical method is rational structure design. Three-dimensional (3D) structures with a high surface-to-volume ratio and abundant active sites can greatly promote the reaction kinetics and facilitate the mass transport [15–17]. However, the atomic utilization efficiency of nanomaterials is generally heavily reduced for the irreversible agglomeration during the catalytic performance, which leads to the serious loss of activity and thus decreased durability [18,19]. Previous studies have shown metal nanoparticles (NPs) can be stabilized by the carbonyl groups (C=O) of cucurbit[6]uril (CB[6]) [20–22]. CB[6] is a rigid pumpkin-shaped macrocyclic molecule with two identical hydrophilic carbonyl-lined portals and a central hydrophobic cavity [23]. The special steric effect provided by macrocyclic molecule CB[6] can be utilized to suppress the overgrowth of Ru nanostructure during the reduction process

* Corresponding authors at: State Key Laboratory of Structural Chemistry, Fujian Institute of Research on the Structure of Matter, Chinese Academy Sciences, Fuzhou 350002, China.
E-mail addresses: mncao@fjirsm.ac.cn (M. Cao), rcao@fjirsm.ac.cn (R. Cao).

https://doi.org/10.1016/j.cclet.2022.07.060
1001-8417/

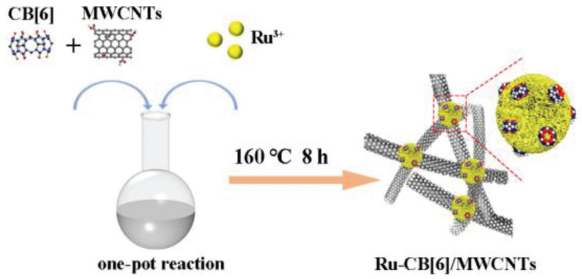

Scheme 1. Illustration of the synthetic process of Ru-CB[6]/MWCNTs.

[24]. Besides, suitable conductive support with excellent electron transport and mass transfer properties also plays a role in fabricating Ru-based HER catalysts [25,26].

Herein, we reported a hierarchically structured nanohybrid composed of well-dispersed flower-like Ru NPs, rigid macrocyclic CB[6] and carboxylated multi-walled carbon nanotubes (MWCNTs) (denoted as Ru-CB[6]/MWCNTs). Taking advantage of the hierarchical structure and the interaction between Ru and CB[6], the as-prepared Ru-CB[6]/MWCNTs catalyst displayed excellent electrocatalytic performance toward HER in a broad pH range. It showed ultra-low overpotential and high electrochemical stability owing to the effective protection of CB[6], which are superior to commercial Pt/C and other HER catalysts.

As illustrated in Scheme 1, Ru-CB[6]/MWCNTs were synthesized *via* a facile wet chemistry approach. Typically, the mixture of $RuCl_3 \cdot 3H_2O$, CB[6] and MWCNT in benzyl alcohol was heated at 160 °C for 8 h in oil after sonication. As the scanning electron microscopy (SEM) image shown in Fig. 1a, well-defined flower-like Ru NPs uniformly dispersed on interlaced carbon nanotubes porous networks. The transmission electron microscopy (TEM) image and size distribution analysis showed that the obtained Ru nanoflowers were evenly distributed with an average size of 50 nm (Fig. 1b and Fig. S1 in Supporting information). The image of single Ru nanoflowers (inset of Fig. 1b) proved that such flowers consist of a vast quantity of nanoparticles which were in cluster form creating the mentioned Ru nanoflowers. Some accessible channels can also be observed, which were conducive to the enhancement of the electrochemical performance by increasing surface area [27]. High-resolution TEM (HRTEM, Fig. 1c) images of Ru-CB[6]/MWCNTs showed clear lattice fringes with *D*-spacing of 0.205 nm and 0.235 nm, corresponding to Ru (101) plane and (100) plane, respectively [28]. And the corresponding fast Fourier transform (FFT, inset of Fig. 1c) pattern matched the electron diffraction pattern of a hexagonal-closed packed Ru [29]. Fig. 1d showed the high-angle annular dark-field scanning TEM (HAADF-STEM) image and corresponding energy-dispersive X-ray spectroscopy (EDX) elemental mapping images, which confirmed that C, N and Ru were distributed on the Ru-CB[6]/MWCNTs surface, consistent with the EDX spectrum (Fig. S2 in Supporting information). These results confirmed the successful synthesis of the Ru-CB[6]/MWCNTs nanocomposite.

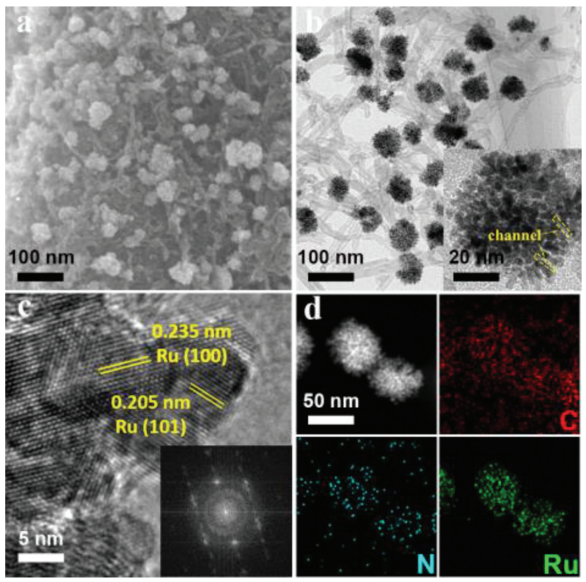

Fig. 1. (a) SEM image, (b) TEM and high-magnification TEM image (inset), (c) HRTEM image and corresponding FFT pattern (inset), (d) HAADF-STEM image and EDX elemental mapping of C, N and Ru of Ru-CB[6]/MWCNTs.

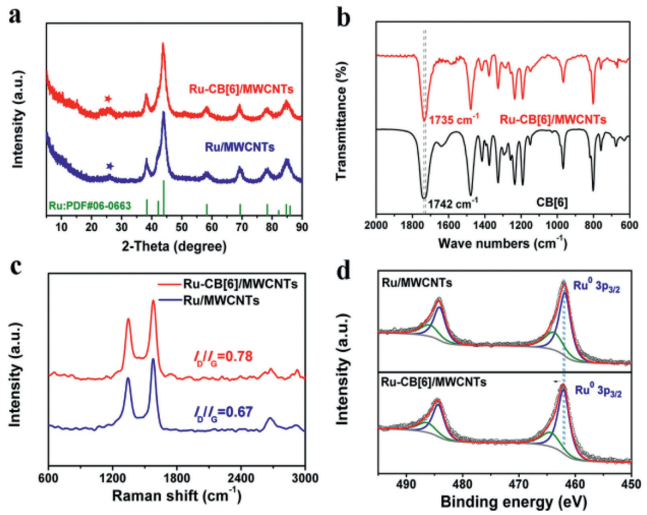

Fig. 2. (a) X-ray diffraction (XRD) pattern of Ru/MWCNTs and Ru-CB[6]/MWCNTs. (b) FT-IR patterns of Ru-CB[6]/MWCNTs and CB[6]. (c) Raman patterns and (d) Ru 3p XPS spectra of Ru-CB[6]/MWCNTs and Ru/MWCNTs.

For comparison, the nanohybrid Ru/MWCNTs and pure Ru NPs were also prepared through a similar synthesis procedure. Pure Ru NPs confronted serious issues of irreversible restacking and severe aggregation (Fig. S3 in Supporting information). However, Ru/MWCNTs showed the same flower-like structure as Ru-CB[6]/MWCNTs (Fig. S4a and b in Supporting information). The presence of carbon nanostructures in Ru/MWCNTs facilitated the formation of nanoflowers in the final structures compared to pure Ru NPs. Different from Ru-CB[6]/MWCNTs, Ru/MWCNTs tended to overgrowth during the synthesis process to form large Ru nanoflowers with diameters of 30–340 nm (Fig. S5 in Supporting information). By comparison of EDX spectrum (Fig. S6 in Supporting information), the *N* element was derived from the macrocyclic molecule CB[6]. These results confirmed that the presence of CB[6] played a vital role in the preparation of highly dispersed flower-like Ru NPs. The volume of 3D structured macrocyclic molecule CB[6] provides a steric effect, which can be utilized to suppress the overgrowth of Ru nanoflowers during the reduction process [30,31].

As the XRD patterns shown in Fig. 2a, the broad diffraction peak at ~25° can be indexed to the (002) plane of MWCNTs [32], while the characteristic peaks located at around 38.4°, 44.0°, 58.3°, 69.4° and 78.4° can be ascribed to the (100), (101), (102), (110) and (103) planes of hcp Ru (PDF#06–0663), respectively. Fourier transform infrared spectroscopy (FT-IR) was used to study the interaction between components. As presented in Fig. 2b, there was a redshift (~7 cm^{-1}) of the C=O peak in Ru-CB[6]/MWCNTs compared to CB[6], indicating the existence of the interaction between the CB[6]

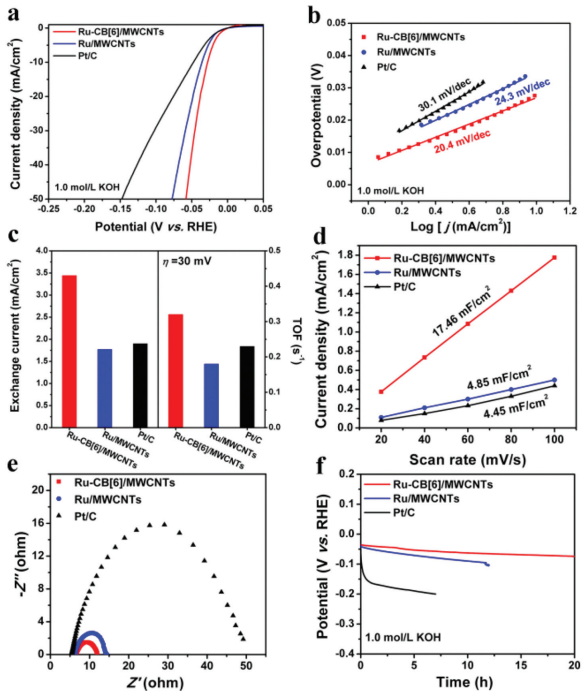

Fig. 3. HER performance of Ru-CB[6]/MWCNTs, Ru/MWCNTs and commercial Pt/C in 1.0 mol/L KOH electrolyte. (a) Polarization curves, (b) Tafel slopes, (c) exchange current density and TOF at the overpotential of 30 mV, (d) the C_{dl}, (e) EIS Nyquist plots at an HER overpotential of 50 mV, and (f) chronopotentiometry curves at the HER current of −10 mA/cm^2.

and Ru [31]. Besides, the ratio of the D and G band intensities (I_D/I_G) usually was employed to analyze the defective structures of the carbon matrix through Raman spectroscopy (Fig. 2c) [32]. The I_D/I_G of Ru-CB[6]/MWCNTs (0.78) was higher than Ru/MWCNTs (0.67), implying that more defects formed on the MWCNTs after introducing CB[6], thus favoring the exposure of more active sites and improving the electrocatalytic performance.

X-ray photoelectron spectroscopy (XPS) analyses of Ru-based catalysts were carried out to explore their compositions and valence states. As observed, the XPS survey spectrum of Ru-CB[6]/MWCNTs (Fig. S7a in Supporting information) indicated the presence of C, O, N and Ru in the catalyst. As shown in Fig. S7b (Supporting information), the peaks at 283.5, 284.8, 286.2, 287.4 and 288.9 eV correspond to C-H, C=C, C=O, C-N and O-C=O, respectively [33]. While the peaks at 280.5 and 284.7 eV belong to metal Ru, corresponding to Ru $3d_{5/2}$ and Ru $3d_{3/2}$, respectively. From the high-resolution spectrum of Ru 3p XPS (Fig. 2d), the Ru^0 $3p_{3/2}$ peak of Ru-CB[6]/MWCNTs showed a shift (0.23 eV) to high binding energy in contrast to that of Ru/MWCNTs, verifying the existence of the electronic interaction between Ru and CB[6]. In addition, the XPS analysis indicated that the percentage of Ru^0 content in Ru-CB[6]/MWCNTs (71.5%) was higher than that of Ru/MWCNTs (67.5%). The high Ru^0 ratio could facilitate H* adsorption to produce Ru-H*, which was beneficial for high electrocatalytic HER activity [34].

The HER performance of Ru-CB[6]/MWCNTs, Ru/MWCNTs and commercial Pt/C (20 wt%) was assessed by a standard three-electrode system. Fig. 3a showed the linear sweep voltammetry (LSV) curves of different catalysts in 1.0 mol/L KOH electrolyte. Ru-CB[6]/MWCNTs required the smallest overpotential (η_{10}) of 27 mV at −10 mA/cm^2, lower than that of Ru/MWCNTs (37 mV) and the Pt/C (47 mV). This result demonstrated that the incorporation of CB[6] into the hierarchically structured catalyst was beneficial to promoting the HER activity. Then the Tafel slope

Table 1
Comparison of HER activities for different electrocatalysts in 1.0 mol/L KOH.

Catalyst	Loading (μg/cm^2)	η_{10} (mV)	Tafel slope (mV/dec)	Refs.
Ru-CB[6]/MWCNTs	20 (Ru)	27	20.4	This work
Ru-CB[6]/rGO	20 (Ru)	48	46.4	[22]
Ru-Mo_2C@CNT	140	15	26	[33]
Ru-OCNT	710	34	27.8	[25]
$RuRh_2$	283	24	31	[36]
Ru/MoO_2	250	16	32	[37]
RuP_2@NPC/CNT	200 (Ru)	12	30	[38]
Ru NCs/BNG	707	14	28.9	[39]
Ru@MWCNT	160	17	27	[28]
Ru-NC-700	200	12	14	[40]
RuCu NDs	35.4 (Ru)	43.4	49	[41]

was extracted from LSV curves to study the HER reaction kinetics of the above catalysts. Ru-CB[6]/MWCNTs had the smallest Tafel slope of 20.4 mV/dec, which was lower than Pt/C (30.1 mV/dec) and Ru/MWCNTs (24.3 mV/dec) (Fig. 3b). Such results suggested a faster HER pathway for Ru-CB[6]/MWCNTs than Pt/C and Ru/MWCNTs, which verified that the hybridization of CB[6] into the composite catalyst promoted the HER activity. According to previous reports, CB[6] could interact with small molecules (such as H_2O and CO_2) through hydrogen-bonding, which is helpful for substrates adsorption and thus improved catalytic activities. Furthermore, exchange current density (j_0) and turnover frequency (TOF) were calculated to reflect the intrinsic catalytic activity of the above catalysts. Ru-CB[6]/MWCNTs had the largest j_0 (3.44 mA/cm^2) compared to Pt/C (1.9 mA/cm^2) and Ru/MWCTs (1.77 mA/cm^2), indicating the superior charge transfer ability between the electrode and the catalyst surface (Fig. 3c, left side). Likewise, Ru-CB[6]/MWCNTs had the largest TOF (0.32 s^{-1}) under an overpotential of 30 mV, which was about 1.39 times Pt/C (0.23 s^{-1}) and 1.78 times Ru/MWCNTs (0.18 s^{-1}), demonstrating the outstanding inherent electrocatalytic efficiency (Fig. 3c, right side). The low overpotential, small Tafel slope, larger j_0 and better TOF of Ru-CB[6]/MWCNTs proved the outstanding HER activity, outperforming commercial benchmark Pt/C catalyst and most recently reported HER catalysts in alkaline conditions (Table 1). To access the electrochemical surface area (ECSA) of the obtained Ru-based catalysts, the cyclic voltammetry (CV) method was carried out to calculate the double-layer capacitance (C_{dl}), which was proportional to the ECSA (Fig. S8 in Supporting information). As shown in Fig. 3d, the C_{dl} of Ru-CB[6]/MWCNTs, Ru/MWCNTs and Pt/C are 17.46, 4.85 and 4.45 mF/cm^2, respectively. This result indicated that introducing CB[6] into the hierarchical composite system generated more active sites, and thus enhanced catalytic activity [35]. Besides, the electrochemical impedance spectra (EIS) was employed to further analyze the HER kinetics. The charge-transfer resistance (R_{ct}) of Ru-CB[6]/MWCNTs, Ru/MWCNTs and Pt/C were 5.7, 8.13 and 43.76 Ω (Fig. 3e, Fig. S9 and Table S1 in Supporting information), respectively. The smallest R_{ct} indicated that Ru-CB[6]/MWCNTs exhibited faster charge transfer owing to the synergistic effect between CB[6] and MWCNTs.

Electrochemical stability is another crucial point for the practical commercialization of catalysts. Chronopotentiometric (CP) tests were carried out to study the durability of the as-prepared Ru catalysts, as well as commercial Pt/C catalyst in 1.0 mol/L KOH electrolyte. As shown in Fig. 3f, Ru-CB[6]/MWCNTs kept 20 h durability test at −10 mA/cm^2 with a slightly increased overpotential. In contrast, the potential dropped 69 mV after the 12 h test for Ru/MWCNTs and 150 mV only after the 7 h test for commercial Pt/C catalyst, respectively. In addition, the LSV curves of Ru-CB[6]/MWCNTs before and after 4000 cycles toward HER were almost overlapped, indicating the superior stability for HER

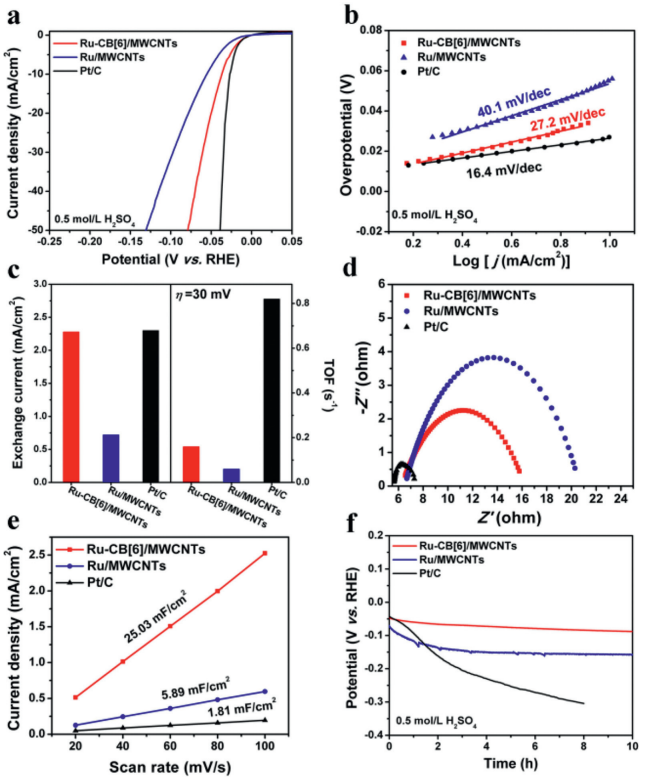

Fig. 4. HER performance of Ru-CB[6]/MWCNTs, Ru/MWCNTs and commercial Pt/C in 0.5 mol/L H_2SO_4 electrolyte. (a) Polarization curves, (b) Tafel slopes, (c) exchange current density and TOF at the overpotential of 30 mV, (d) EIS Nyquist plots at an HER overpotential of 50 mV, (e) the C_{dl}, and (f) chronopotentiometry curves at the HER current of -10 mA/cm^2.

in alkaline electrolyte (Fig. S10a in Supporting information). For commercial Pt/C, the overpotential (at -10 mA/cm^2) dramatically increased from 47 mV at the first cycle to 83 mV at the 4000th cycle (Fig. S10b in Supporting information) due to the weak interaction between Pt and C substrate. Furthermore, TEM image of Ru/MWCNTs after durability test showed severe aggregation (Fig. S11 in Supporting information), while the structure and size of Ru-CB[6]/MWCNTs were well maintained after 20 h test (Fig. S12 in Supporting information), which confirmed the good protection effect for the flower-like Ru NPs of CB[6].

The HER performance of Ru-CB[6]/MWCNTs was also investigated in 0.5 mol/L H_2SO_4 electrolyte. Ru-CB[6]/MWCNTs showed an overpotential of only 37 mV at -10 mA/cm^2 and a small Tafel slope of 27.2 mV/dec, which is lower than that of Ru/MWCNTs (57 mV, 40.1 mV/dec) and comparable to that of commercial Pt/C (27 mV, 16.4 mV/dec) (Figs. 4a and b). This result also suggested that the introduction of CB[6] was beneficial to the HER kinetic for Ru-based electrocatalysts. Moreover, the large j_0 of Ru-CB[6]/MWCNTs suggested the high intrinsic HER activity, which was also demonstrated by the TOF of Ru-CB[6]/MWCNTs at the overpotential of 30 mV (Fig. 4c). As conducted in Fig. 4d and Table S2 (Supporting information), the R_{ct} of Ru-CB[6]/MWCNTs was much lower than that of Ru/MWCNTs, indicating a faster electron transfer at the interface of Ru-CB[6]/MWCNTs electrode and electrolyte due to the introduction of CB[6]. The C_{dl} of Ru-CB[6]/MWCNTs, Ru/MWCNTs and commercial Pt/C were 25.03, 5.89 and 1.81 mF/cm^2 (Fig. 4e and Fig. S13 in Supporting information), respectively, suggesting the most abundant active sites on Ru-CB[6]/MWCNTs. As shown in Fig. 4f, Ru-CB[6]/MWCNTs exhibited enhanced stability with a slight overpotential increase after 10 h test at -10 mA/cm^2 compared with Ru/MWCNTs, while Pt/C exhibited much poorer stability after 8 h test. The TEM image of Ru-CB[6]/MWCNTs after the 10 h stability test showed no change in the morphology (Fig. S14 in Supporting information). These results demonstrated that Ru-CB[6]/MWCNTs exhibited favorable electrochemical performance as a highly active and stable catalyst for acidic HER, which also outperformed many other HER catalysts reported previously in acidic media (Table 2). Given the price is far lower for Ru compared to Pt, Ru-CB[6]/MWCNTs is a promising alternative to commercial Pt/C for HER in acidic electrolyte.

Table 2
Comparison of HER activities for different electrocatalysts in 0.5 mol/L H_2SO_4.

Catalyst	Loading (μg/cm^2)	η_{10} (mV)	Tafel slope (mV/dec)	Refs.
Ru-CB[6]/MWCNTs	20 (Ru)	37	27.2	This work
$RuRh_2$	283	34	17	[36]
RuNi/CQDs-600	5.94 (Ru)	58	55	[42]
Ru@MWCNT	81.2 (Ru)	13	27	[28]
Ru-RuO_2/CNT	800	63	31	[43]
Ru_2P/graphene	1×10^3	18	32	[44]
Ru SAs@PN	3.3 (Ru)	24	38	[45]
RuCoP	53.1 (Ru)	11	31	[46]
C_3N_4-Ru-F	153	140	57	[47]

Ru-CB[6]/MWCNTs catalyst also exhibited a comparable electrochemical performance in 1.0 mol/L PBS electrolyte. In Figs. S15a and b (Supporting information), Ru-CB[6]/MWCNTs showed an overpotential of only 70 mV at a current density of -10 mA/cm^2 and a small Tafel slope of 57.1 mV/dec, which were comparable to Pt/C (49 mV, 46.8 mV/dec) and surpassed most of the recently reported materials (Table S3 in Supporting information). The catalyst stability was examined and the potential at -10 mA/cm^2 was recorded for 12 h by the chronopotentiometry test, showing the superior long-term stability of Ru-CB[6]/MWCNTs for HER in 1.0 mol/L PBS electrolyte (Fig. S15c in Supporting information).

In summary, a hierarchically structured Ru nanocomposite was successfully synthesized by a simple wet chemical method for HER. A variety of characterization and tests showed that the unique hierarchical structure and the interaction between Ru nanoparticles and CB[6] of Ru-CB[6]/MWCNTs composite led to good electronic conductivity and abundant active sites, which boosted its electrocatalytic HER activity and stability. Ru-CB[6]/MWCNTs required overpotentials of 27, 37 and 70 mV at -10 mA/cm^2 in alkaline, acid, and neutral electrolytes, respectively. Therefore, the as-prepared Ru-CB[6]/MWCNTs electrocatalyst can be regarded as a cheaper and more promising alternative to Pt-based catalysts for further electrocatalytic HER.

Declaration of competing interest

The authors declare that they have no known competing financial interests or personal relationships that could have appeared to influence the work reported in this paper.

Acknowledgments

We appreciate the financial support from the National Key R&D Program of China (Nos. 2017YFA0206802, 2018YFA0704502); the National Natural Science Foundation of China (NSFC, No. 22033008). Fujian Science & Technology Innovation Laboratory for Optoelectronic Information of China (No. 2021ZZ103).

Supplementary materials

Supplementary material associated with this article can be found, in the online version, at doi:10.1016/j.cclet.2022.07.060.

References

[1] E. Wang, S. Zhang, J. Li, ChemElectroChem 7 (2020) 4526–4534.
[2] Z.J. Chen, X.G. Duan, W. Wei, et al., Nano Res. 13 (2020) 293–314.
[3] L.Y. Zhang, Y.J. Zheng, J.C. Wang, et al., Small 17 (2021) 2006730.
[4] J. Yu, Q.J. He, G.M. Yang, et al., ACS Catal. 9 (2019) 9973–10011.
[5] D.S. Wu, K. Kusada, S. Yoshioka, et al., Nat. Commun. 12 (2021) 1145.
[6] C. Wang, L.M. Qi, ACS Mater. Lett. 3 (2021) 1695–1701.
[7] M.N. Cao, D.S. Wu, R. Cao, ChemCatChem 6 (2014) 26–45.
[8] T. Wang, P. Wang, Y. Pang, et al., Nano Res. 15 (2022) 3946–3951.
[9] Y.M. Shi, B. Zhang, Chem. Soc. Rev. 45 (2016) 1529–1541.
[10] L. Zhang, J. Zhu, X. Li, et al., Interdisciplinary Mater. 1 (2022) 51–87.
[11] J.J. Wang, X.Y. Yue, Y.Y. Yang, et al., J. Alloys Compd. 819 (2020) 153346.
[12] Y.H. Zhu, P.F. Tian, H.L. Jiang, et al., CCS Chem. 3 (2021) 2539–2547.
[13] Y.T. Li, F.Q. Chu, Y. Liu, et al., Chem. Commun. 54 (2018) 13076–13079.
[14] S.Y. Bae, J. Mahmood, I.Y. Jeon, et al., Nanoscale Horiz. 5 (2020) 43–56.
[15] D. Cao, J.Y. Wang, H.X. Xu, et al., Small 16 (2020) 2000924.
[16] M.Y. Yuan, H. Xu, Y. Wang, et al., ChemElectroChem 7 (2020) 3135–3139.
[17] T. Wang, P. Wang, W. Zang, et al., Adv. Funct. Mater. 32 (2021) 2107382.
[18] H. Li, M.T. Zhang, L.C. Yi, et al., Appl. Catal. B: Environ. 280 (2021) 119412.
[19] F. Zhang, Y. Zhu, Y. Chen, et al., J. Mater. Chem. A 8 (2020) 12810–12820.
[20] M.N. Cao, D.S. Wu, S.Y. Gao, et al., Chemistry 18 (2012) 12978–12985 (Easton).
[21] M.N. Cao, D.S. Wu, W.P. Su, et al., J. Catal. 321 (2015) 62–69.
[22] Z.W. Gong, D.S. Wu, M.N. Cao, et al., Chem. Commun. 56 (2020) 9392–9395.
[23] J. Lagona, P. Mukhopadhyay, S. Chakrabarti, et al., Angew. Chem. Int. Ed. 44 (2005) 4844–4870.
[24] R.R. Chen, M.N. Cao, W.G. Yang, et al., Chem. Commun. 55 (2019) 9805–9808.
[25] R.F. Ding, L.J. Lin, C.G. Pei, et al., Chemistry 27 (2021) 11150–11157 (Easton).
[26] M. Khan, A.B. Yousaf, M.M. Chen, et al., Nano Res. 9 (2016) 837–848.
[27] Y. Li, Y. Guo, S.F. Yang, et al., ACS Appl. Mater. Interfaces 13 (2021) 5052–5060.
[28] D.H. Kweon, M.S. Okyay, S.J. Kim, et al., Nat. Commun. 11 (2020) 1278.
[29] J. Mahmood, F. Li, S.M. Jung, et al., Nat. Nanotechnol. 12 (2017) 441–446.
[30] D.S. Wu, M.N. Cao, R. Cao, Nano Res. 12 (2019) 2628–2633.
[31] H.H. You, D.S. Wu, Z.N. Chen, et al., ACS Energy Lett. 4 (2019) 1301–1307.
[32] W. Wang, T. Yuan, H.T. Tang, et al., Chem. Phys. Lett. 779 (2021) 138879.
[33] X.K. Wu, Z.C. Wang, D. Zhang, et al., Nat. Commun. 12 (2021) 4018.
[34] J. Wang, Z.Z. Wei, S.J. Mao, et al., Energy Environ. Sci. 11 (2018) 800–806.
[35] Z.X. Yang, R. He, H.M. Wu, et al., Int. J. Hydrogen Energy 46 (2021) 9690–9698.
[36] X.Q. Mu, J.N. Gu, F.Y. Feng, et al., Adv. Sci. 8 (2021) 2002341.
[37] H.J.W. Li, K. Liu, J.W. Fu, et al., Nano Energy 82 (2021) 105767.
[38] F. Zhou, R.J. Sa, X. Zhang, et al., Appl. Catal. B: Environ. 274 (2020) 119092.
[39] S.H. Ye, F.Y. Luo, T.T. Xu, et al., Nano Energy 68 (2020) 104301.
[40] B.Z. Lu, L. Guo, F. Wu, et al., Nat. Commun. 10 (2019) 631.
[41] K. Gao, Y. Wang, Z.W. Wang, et al., Chem. Commun. 54 (2018) 4613–4616.
[42] Y. Liu, X. Li, Q.H. Zhang, et al., Angew. Chem. Int. Ed. 59 (2020) 1718–1726.
[43] M.T. Zhang, J.X. Chen, H. Li, et al., Nano Energy 61 (2019) 576–583.
[44] T.T. Liu, J.M. Wang, C.Y. Zhong, et al., Chemistry 25 (2019) 7826–7830 (Easton).
[45] J. Yang, B.X. Chen, X.K. Liu, et al., Angew. Chem. Int. Ed. 57 (2018) 9495–9500.
[46] J.Y. Xu, T.F. Liu, J.J. Li, et al., Energy Environ. Sci. 11 (2018) 1819–1827.
[47] Y. Peng, B.Z. Lu, L.M. Chen, et al., J. Mater. Chem. A 5 (2017) 18261–18269.